Detailing patient specific modelling to aid clinical decision-making

Richmond, S., Al Ali, A. M., Beldie, L., Chong, Y. T., Cronin, A., Djordjevic, J., Drage, N. A., Evans, D. M., Jones, D., Lu, Y., Marshall, D., Middleton, J., Parker, G., Paternoster, L., Playle, R. A., Popat, H., Rosin, P. L., Sidorov, K., Toma, A. M., Walker, B., Wilson, C. and Zhurov, A. I.

Detailing patient specific modelling to aid clinical decision-making

Richmond S, Al Ali AM, Beldie L, Chong YT, Cronin A, Djordjevic J, Drage NA, Evans DM, Jones D, Lu Y, Marshall D, Middleton J, Parker G, Paternoster L, Playle RA, Popat H, Rosin PL, Sidorov K, Toma AM, Walker B, Wilson C, Zhurov AI.

Subtle facial differences make an individual unique and it is this uniqueness that needs to be recognized, defined, categorised and incorporated into a computerized patient specific model. The craniofacial structures are complex and there are many clinical and non-clinical specialties that have a specific interest in the dental and oro-facial region. Although there have been significant investments in research to explain development and facial variation, the mechanisms of how normal and abnormal growth/facial development occurs still remains unclear and subject to many theories. Improving knowledge in how the facial tissues arise and function will enhance the validity of computerized models. The aim of this chapter is to highlight advancements that have led to characterization of facial tissues and how these can be utilized and refined for computerized models to aid clinical decision-making.

This chapter will address the progress made so far in determining a patient specific model in terms of:

- Acquisition of facial data
- Genetic and non-genetic factors contributing to facial variation
- Modelling facial structures based on average estimates for surgical planning and simulation
- Methods to determine facial movement pre and post-surgical intervention
- On-going refinement of techniques:
  Registration
  Determination of the orientation of facial muscle fibres

Acquiring facial data

To model or visualise living anatomical structures it is important to capture clinical data in a non-destructive way. Over the last 40 years there have been significant advances in imaging techniques, which have enabled visualisation and reconstruction of the living internal organs, which previously were only visible by operation or by dissection. Static images of structures have been invaluable but more recently it has been realised that observing structures during function has added benefit, for example, cardiac magnetic resonance imaging to evaluate cardiac function (Hundley et al, 2010) and videofluoroscopy to study swallowing impairment in patients with neurological impairment (Kang et al, 2011).

Therefore to develop a patient specific model to aid clinical decision making for the head and neck

we need not only information on the constitutive components on the head and neck but we also need imaging techniques to record and model the internal structures during rest and also undergoing a range of functions. In addition it is important to diagnose craniofacial anomalies based on normal variation and plan the surgery necessary to normalise any facial disharmony if required.

Every person has a unique soft tissue and skeletal facial structure and these structures are complex and require a variety of techniques to capture the full depth of facial tissues. For surface scanning, static or video-imaging techniques are used (laser or photogrammetric techniques) (Kau, 2010). To capture the detail of the skeletal framework computed tomography (CT), Cone Beam Computed Tomography (CBCT) and Magnetic Resonance Imaging (MRI) can be applied (Drage and Rout, 2010). To capture the detail of the underlying soft tissues (e.g. muscle and brain) techniques such as MRI, CT and ultrasound are required. Examples of the images obtained from the image capture machines are shown later in the text. Specialised techniques have been developed to identify muscle fibre orientation such as diffusion weighted imaging. Capturing any facial data is complex and the data requires validation as certain capture techniques are subject to distortion due to variation in image uniformity (Bryant et al, 2008) and relative spatial position of these structures that make up the face (e.g. surface air interface in CT and MRI).

Genetic and non-genetic factors contributing to facial variation

The relative proportions of genetic and non-genetic factors contributing to dentofacial variation has evoked strong debate (Lundström, 1984). Quantifying the heritability of craniofacial features is a prerequisite for understanding normal craniofacial development and elucidating how abnormal pathology arises. Evidence from twin, family and animal studies has suggested that much of the variation in craniofacial features is heritable (Kohn, 1991), although the majority of studies have involved small sample sizes, and/or less than ideal study designs. For example, most of the larger studies in craniofacial development have involved parent-offspring designs, which cannot distinguish between common environmental and genetic sources of variation, and thus may produce inflated estimates of the underlying heritability.

With the advent of molecular genetic techniques over the past thirty years, attention has now turned to identifying the individual genes influencing craniofacial development. In this respect, mutation bearing genes have been identified for over 340 syndromes associated with oral facial clefts, and numerous candidate genes have been implicated by allelic association and linkage analyses (Cohen, 2002). Whilst considerable advances have been made in elucidating the genetic basis of pathological conditions, the identity of individual genetic variants which affect normal craniofacial development in population based samples are largely unknown. However, a recent genome-wide association study of normal facial morphology in 2,185 15-year-old children found a

robustly replicated association between a SNP in PAX3 (rs7559271) and the nasion to mid-endocanthion distance (n-men) (Evans, et al, 2011). Although genetic studies of normal craniofacial variation are in their infancy, it is hoped that the insights they provide will inform clinicians on how the face develops and reacts to surgical interventions.

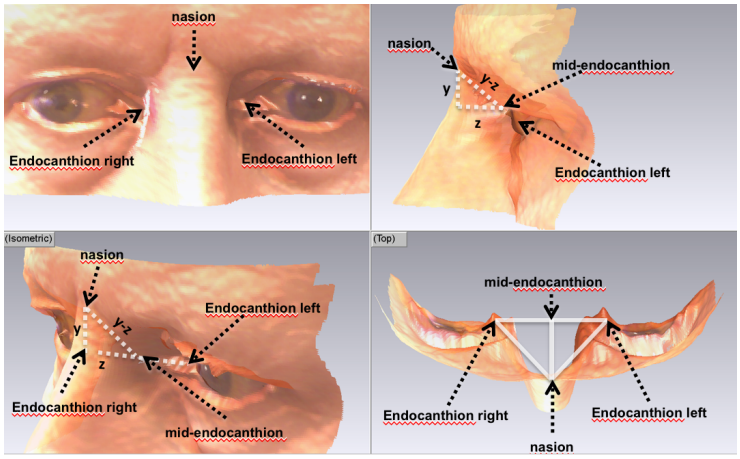

Figure 1 Showing construction of the nasion to mid-endocanthion distance associated with the PAX3 gene.

There are many other factors that can affect facial variation such as the age of the individual, ethnicity, gender and environment. In a study of facial variation in 4747 children of the same age (15-years-old), 82 percent of variation could be explained by 14 principal components (Toma, et al, 2011). The first 3 components explained 46% of variation. These components were face height (28.8%), inter eye distance (10.4%) and nose prominence (6.7%) (Figure 2).

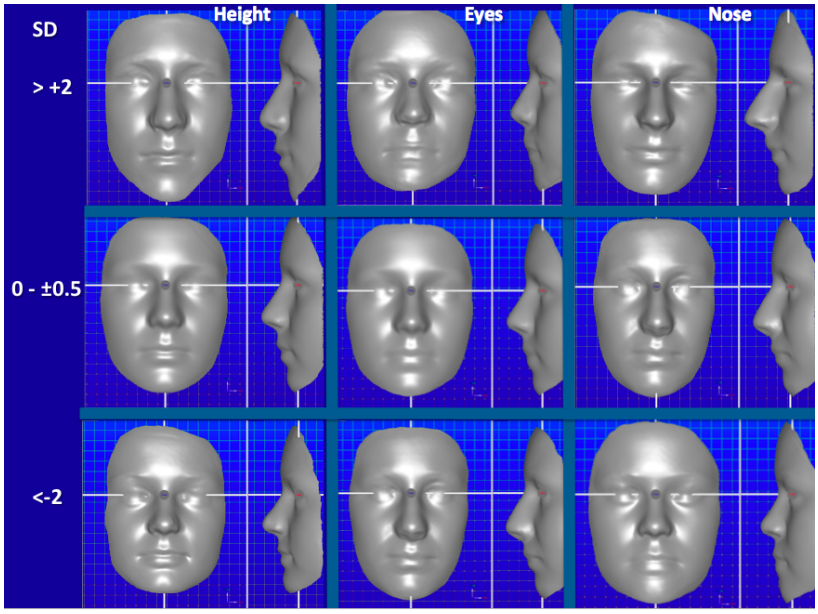

Figure 2 Facial variation: Left column showing variation from long face (top) to short face (bottom); middle column eyes further apart (top) and eyes closer together (bottom) and right column large nose (top) to small nose (bottom).

Significant facial variations have been highlighted between five different ethnic populations for

example similarities in facial shapes were identified between females in Wales and Hungary but less concordance with females in Wales and the USA (Kau et al, 2010). The face changes throughout life, increasing in size and changing shape. Puberty is when key facial differences between the sexes become defined (Figure 3). Males tend to develop prominent noses and chins, with flatter infra-orbital regions than females between 12 and 17 years of age. Females tend to reach puberty 12 to 14 years of age and males 14 to 16 years of age. Subtle facial changes occur throughout life as the individual ages.

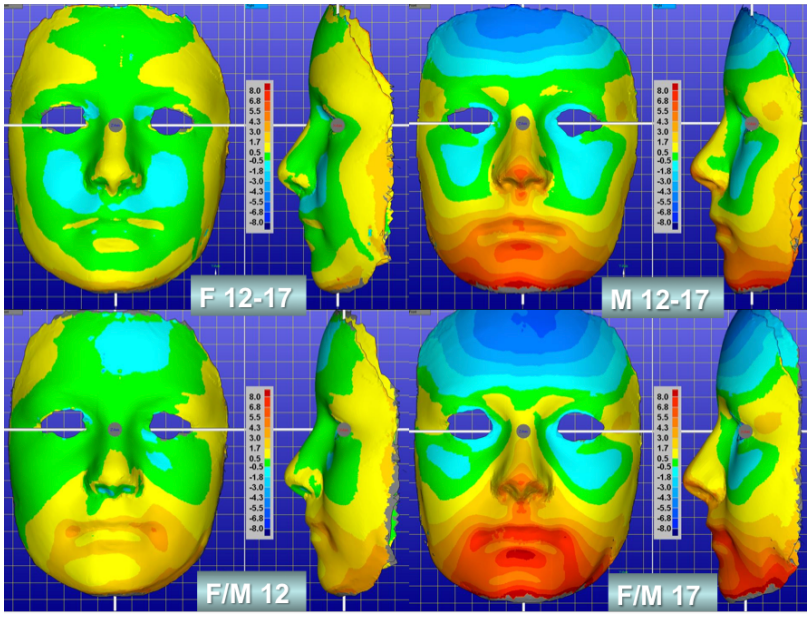

Figure 3 Colour maps showing differences between females and males between 12 and 17 years of age: Females (top left), males (top right), females and males aged 12 (bottom left) and females and males at 12 years of age (bottom left) and at 17 years of age (bottom right). Cooler colours (light and dark blues) show negative distances and warmer colours (oranges and reds) positive distances. Male chins and noses grow significantly forward from age 12 to 17 years of age.

There have been a few studies assessing the influence of medical conditions on facial variation. In a study of insulin sensitivity in 2181 white 15-year-old children (1027 males, 1154 females) the first two principal components (facial height and inter-eye distance) were significantly, though weakly, associated with insulin sensitivity. The average face of males with low insulin sensitivity was wider (up to 3.24 mm) with a shorter nose and less protrusive lips (up to 2.26 mm) compared with the average face of males with high insulin sensitivity. The average face of females with low insulin sensitivity was also wider, with a more protrusive chin (up to 1.71 mm), shorter nose and less protrusive lips (up to 1.28 mm) compared with the average face of females with high insulin sensitivity (Djordjevic et al, 2010).

A further study of the influence of asthma on facial development was conducted in 471 children who had been diagnosed as asthmatic at 91 months of age (Henderson et al, 2008). The facial parameters were assessed against a control of 1637 healthy children. The inter ala distance

(width of the nose) was 0.1mm wider and mid-face height was 0.4mm shorter in asthmatic females compared with non-asthmatic females. No facial differences were detected in males.

These few examples have shown that facial size and shape can be influenced by genetic and environmental influences. There are a wide variety of shapes and sizes of cheeks, chins, noses and lips and as a consequence will grow differently and respond differently to surgical interventions.

Modelling facial structures based on average estimates for surgical planning and surgical simulations

It has been traditional for the assessment of facial discrepancies to be compared with average estimates for the normal population. This is undertaken on relatively small population groups usually between the ages 12 to 18 years of age (Riolo et al, 1979; Bhatia and Leighton, 1993). There are relatively few repositories for 3D facial analyses. A significant proportion of facial evaluations have been dependent on 2D cephalometric analyses and out-dated subjective assessments. Although these assessments are helpful they do not characterise the numerous permutations and associations of facial characteristics.

To date it is possible to acquire an accurate 3D facial shell (static and dynamic) using laser scanners or by photogrammetric techniques and skeletal topography using CBCT. It has been challenging to acquire detail of the underlying tissues (fascia, fat, nerves, blood vessels and muscles) lying between the facial surfaces and underlying bone. One possible solution is to apply average data acquired from forensic reconstruction (Richmond et al, 2010). The muscles can be fashioned and placed in the approximate anatomical positions (Figure 4).

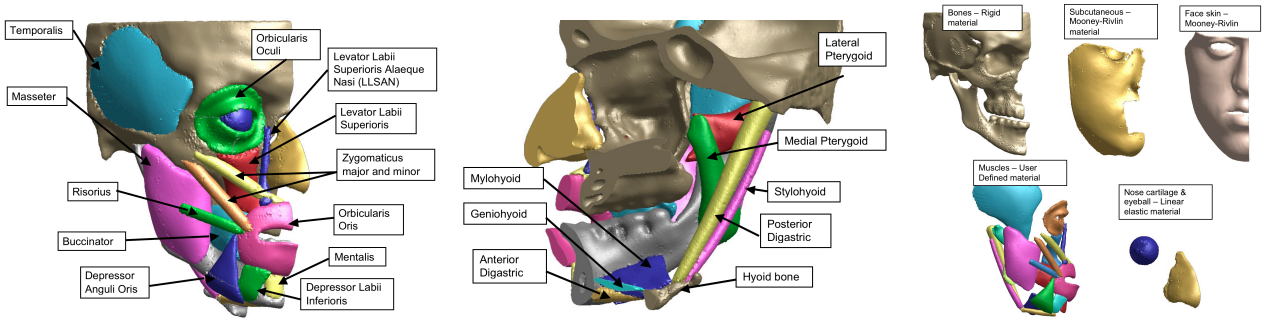

Figure 4 The positioning of muscles on a segmented facial skeleton obtained from a CBCT (Left and middle). The facial tissues can be modelled: Bone – rigid; Subcutaneous fat and skin – Mooney/Rivlin; Muscles – user defined; Nose cartilage/eyeball – linear elastic (right).

A finite element model was created using Simpleware® (Simpleware Ltd., 2008) and Oasys.PRIMER (Oasys Ltd & Arup, 2009). The material properties for different components were given as: the skeletal structure –rigid; subcutaneous – Neo-Hookean; facial skin, nose cartilage and eyeballs – linear elastic; facial muscles – user defined materials or linear elastic (Figure 4)

(Beldie et al, 2010). For the finite element model to produce valid predictions, an accurate constitutive model of the muscles is critical (Richmond et al, 2010). The constitutive muscle model was formulated based on Hill's one-dimensional model and can be described as active, quasi-incompressible, fibre reinforced and hyperelastic (Hill, 1938). The model was validated against experimental data under passive and active elongation simulations and was proved to be capable of simulating active and passive behaviour (Lu et al, 2011). The constitutive model was implemented into LS-DYNA (Livermore software technology corporation, 2007) through user-defined material (UMAT) and utilised to simulate facial expressions. Facial expressions were achieved by activating the facial muscle groups. For example disgust was achieved by stimulating the levator labii superioris alaeque nasi, orbicularis oculi and depressor anguli oris muscles simultaneously and smiling was achieved by activating the orbicularis oculi, zygomaticus minor and zygomaticus major muscles simultaneously (Figure 5).

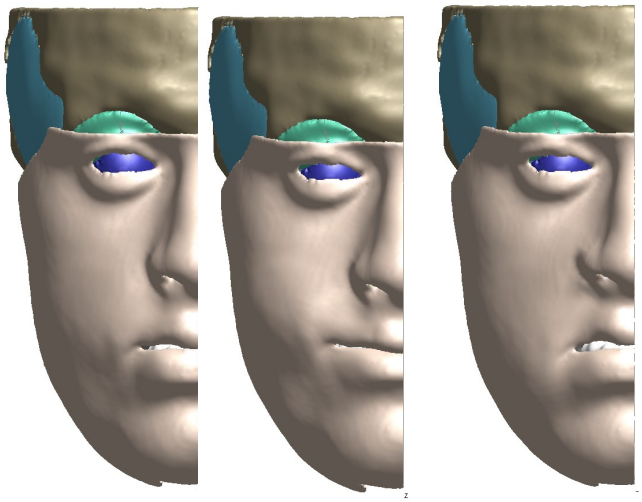

Figure 5. Facial expressions rest (left), smiling (middle) and disgust (right)

Surgical planning and simulation

A 20-year-old patient expressed an interest in improving his appearance by reducing the prominence of his chin. At his first appointment full records were taken and the plan was to align his teeth prior to surgery. Once his teeth were aligned a surface facial laser scan (with colour texture) and a CBCT was performed. The surface scan was fitted to the surface of the CBCT 3D construction. An average facial template for an 18 to 22-year-old male was fitted to the patients facial shell using best-fit with both shells aligned to the mid-intercanthal line (Zhurov et al, 2010). A colour deviation map was used to highlight differences between the individual and the average face (Figure 6). The patient's cheeks showed a deficiency of 5mm although the chin was in a similar anterior-posterior position and the facial height was 3 to 4mm longer than the average male. Analysing these data it was decided to move the maxilla upwards by 4mm and forwards by 5mm. The movement of the maxilla will correct the mid-face discrepancy. The mandible was moved to

the best-fit of the upper and lower teeth. Achieving the best occlusal interdigitation was a priority although by doing this it was recognised that the position of the chin would be less prominent than the average face. The relationship of the soft tissues to the hard tissues have changed substantially pre- and post-operatively (Figure 7). The finite element predictions showed a very similar outcome to that achieved with small areas of discrepancy at 3 and 6 months. The green areas indicate that the surgical prediction was generally within 0.8mm of the actual surgical correction (Fig. 7).

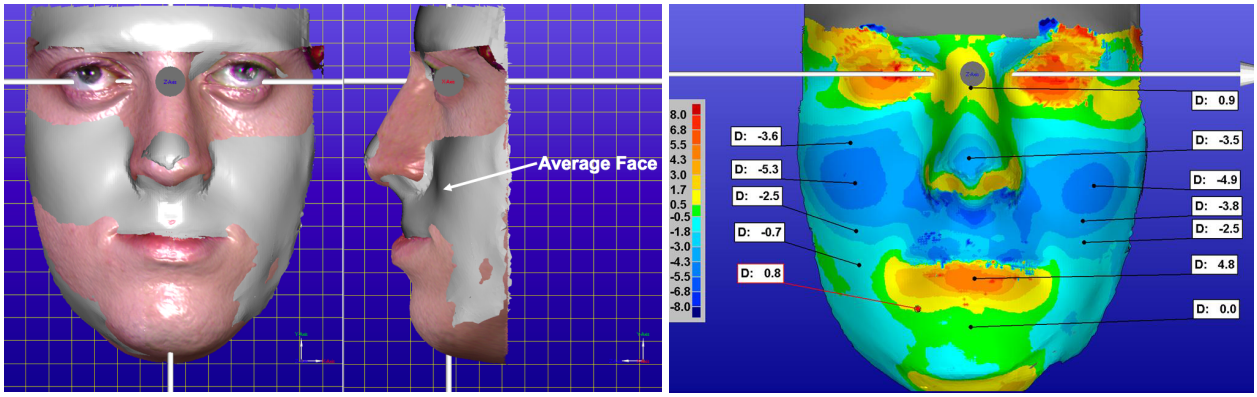

Figure 6 Colour textured image overlaid on average face for males 18 to 22 years of age (left); colour deviation map of patient compared with a facial average highlighting a deficiency in the middle part of the face by 5mm (right).

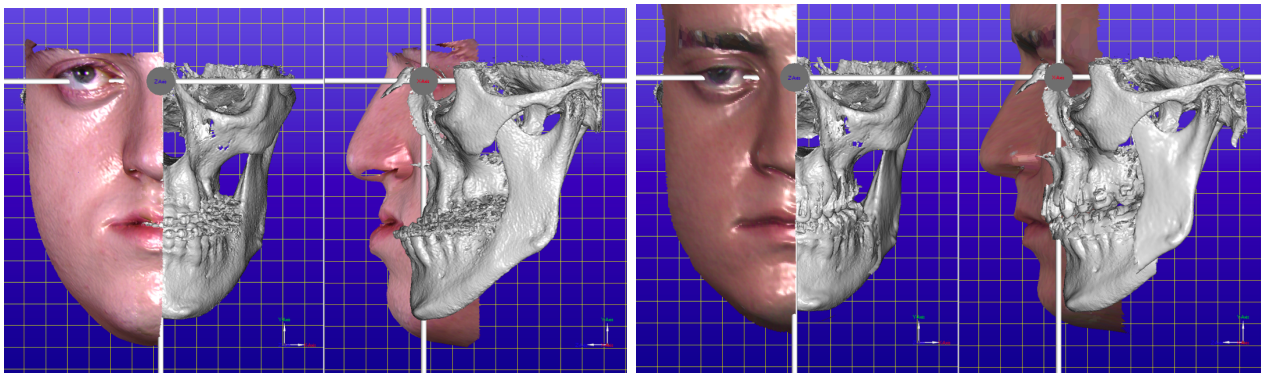

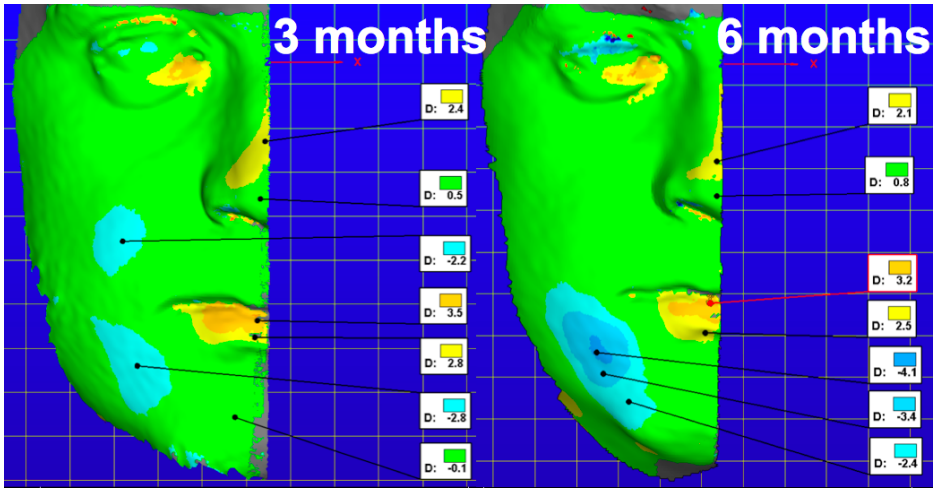

Figure 7 Pre-surgical (top left) and post-surgical plan (top right). 3 month and 6 month post

surgical evaluation of the surgical plan and actual outcome. There is a high level of concordance between the surgical plan and surgical outcome at 3 and 6 months (green represents difference of less than 0.8mm). Greater errors were particularly associated with the lower lip (3.5mm). This reconstruction was undertaken on static images but it is also important to evaluate facial changes during normal function (speech, expressions and mastication).

Methods to determine facial movement pre and post-surgical intervention

Our facial appearance and expressive behaviours have a major impact on how we are perceived and how others in society perceive us. The inability to express oneself via facial movement can have serious social consequences as both verbal and non-verbal movements communicate our emotional state of mind to others. Such patients who may be affected include those with facial nerve paralysis, those with dentofacial deformities and patients with cleft lip. Many of these patients will opt to have reconstructive or orthognathic surgery to correct their aesthetic and functional deficits. It is important that there are adequate measures for objectively quantifying pre- and post-operative function for these patients as this will help in diagnosing the severity of the impairment and aid in outcome assessment (Nooreyazdan et al, 2004, Mishima et al, 2009, Okudaira et al, 2008).

The first consideration in facial movement analysis pre- and post-operation is what facial gesture is most appropriate to use to measure movement. The choice of action can broadly be classified into verbal and non-verbal facial gestures (Popat et al, 2011). In principle, any facial gestures can be employed for the assessment of facial movement. However facial gestures that may be appropriate for use in psychology assessments for example may not be so for assessment in pre- and post-operation. One must therefore consider the application carefully.

In addition, when monitoring facial movement over time or through intervention the measure of facial movement used should be repeatable. If this is not the case, then individual variation or difference in the performed facial gesture between two time points will induce error into the assessment. Verbal facial gestures tend to exhibit higher reproducibility when compared to facial expressions (Popat et al, 2010).

Data analysis

Research into facial movement utilises statistical modelling techniques to analyse the dynamic 3D data acquired. A sequence of facial movement may typically contain a set of 3D images at 30-60 frames per second (Figure 9).

Figure 9 Selected sequential frames of a patient saying the word /rope/

Images from the sequence must be registered within the same 3D space. This allows valid comparison of facial movement between frames from within a sequence but also between different groups and time points. Using 3D facial landmarks, the coordinates of interest can then extracted from images along the timeline to form the dataset. Landmark trajectories can be plotted and inter-landmark distances measured to give information on facial movement pre- and post-operation to assess functional change. To explore variability in facial shape however and isolate patterns/relationships between the areas of facial movement more sophisticated methods of modelling are required such as Principal Component analysis (PCA).

Here we illustrate a patient with a prominent chin who was part of a cohort that underwent orthognathic surgery to both upper and lower jaws. The change in lip movement pre- and post-operation is statistically modelled using the x, y and z coordinates of 6 anthropometric landmarks: labiale superius (ls) - the midpoint of the upper vermilion line, labiale inferius (li) – the midpoint of the lower vermilion line, crista philtri (cph L/R) – the point on the left and right elevated margins of the philtrum above the vermilion line and cheilion (ch L/R) – the point located at the left and right labial commissure (Farkas, 1993). Data of the patient saying several words were acquired immediately pre- and 6 months post-operation using a 3D motion capture system (Figure 10).

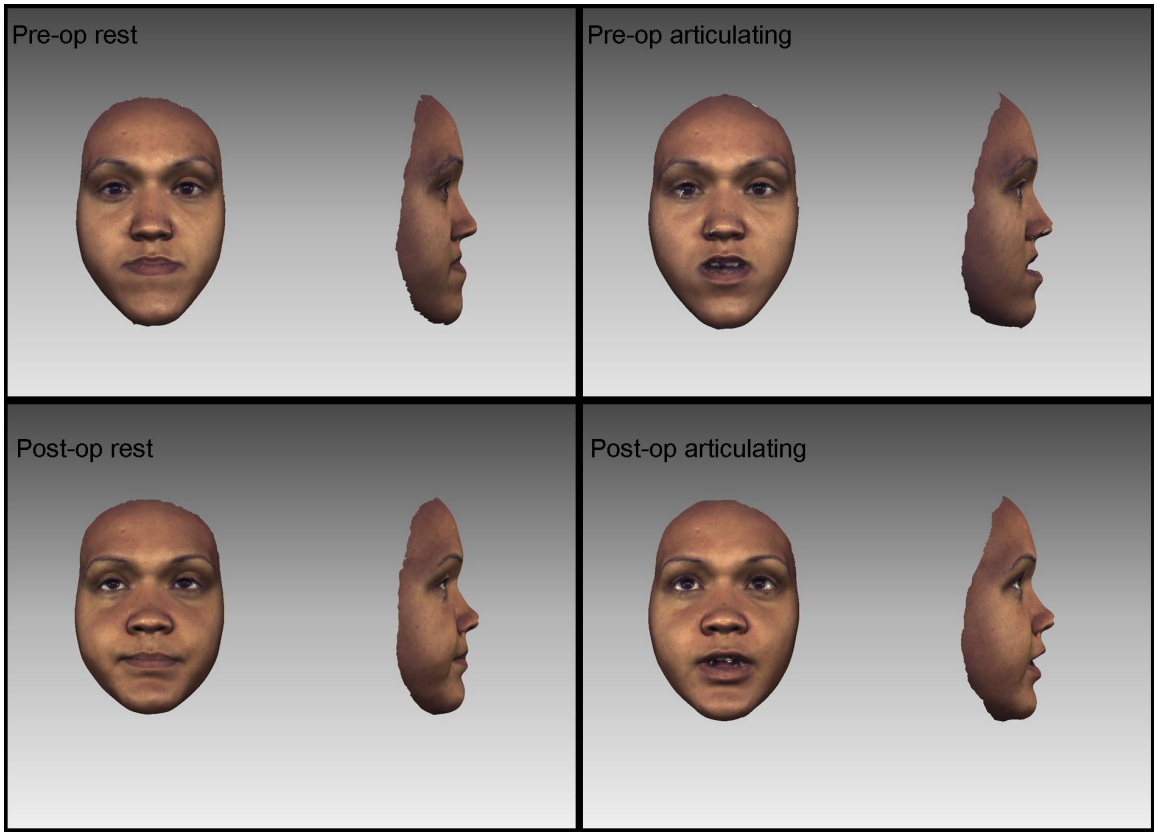

Figure 10 Patient with a severe Class 3 dentofacial deformity pre- and post-operation at rest and articulating the word /rope/

The 3D facial shells at rest and at maximum displacement for each word both pre- and post operation were registered (aligned) in space using Generalised Procrustes Analysis by removing translation and rotation (Dryden and Mardia, 1998). Scaling was not incorporated to preserve lip size and shape. The mean position of each landmark (centroid) was plotted with 2 standard deviations to give a 3D ellipsoid representing 95 percent of the variation in lip shape for each time point. Figure 11 shows the difference in lip shape for the group from pre- to post-operation. Post-operation the mean lip height has been reduced and the mean lip width increased.

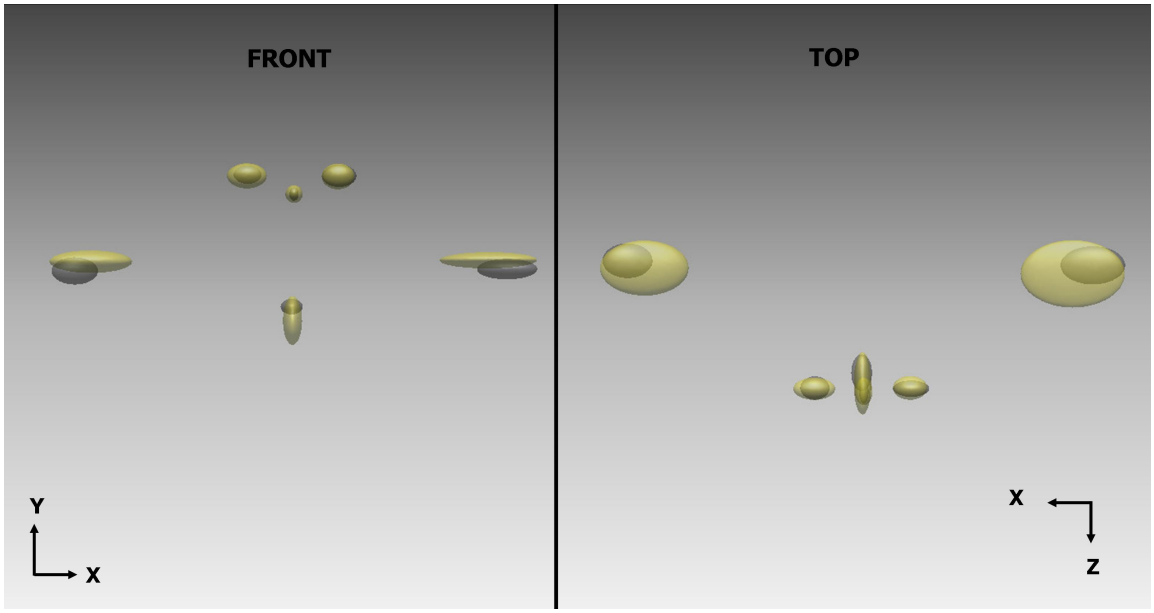

Figure 11 3D ellipsoid plot (mean ± 2 SD) showing the difference in lip shape pre- and post-operation (pre- yellow, post- black)

The effect of this on lip movement can be visualised in Figure 12 where 3D ellipsoids have been used to plot pre- and post-operation movement for the word /rope/ against a control or average group. Post-operation, there is less protrusion and more downward movement of the corners of the mouth, which when compared with the control group shows that both the dentofacial aesthetics and function have been normalised (Figure 12).

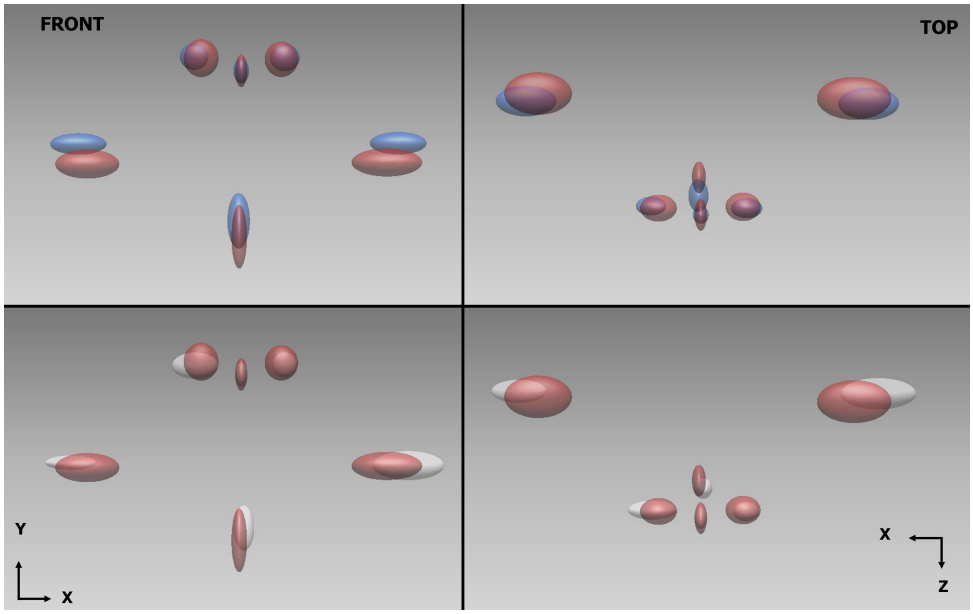

Figure 12 3D ellipsoid plot (mean ± 2 SD) showing lip shape for maximum articulation of the word /rope/ comparing normal movement (red) to pre-operation (blue) and post-operation (white)

Figure 12 Pre- and post-operation facial appearance. Surgery has brought the maxilla forwards and moved the mandible backwards enabling an excellent interdigitation of the upper an lower dentitions.

Although treatment aims for patients have always been to restore aesthetics and function, traditionally methods to monitor facial function has lacked precision and objectivity. With 3D motion capture systems, statistical modelling techniques are a valuable technique in processing large volumes of data resulting in a concise and meaningful interpretation of facial function.

Tracking movement of the mandible

Although surface movement is important for daily interactions it is also necessary to reliably record movement of the mandible also during function and especially prior to surgical planning. There have been several methods employed in the past such as the photography (Wood, 1979), Kinesiograph (Martin et al, 2000) and radiographic (Kim et al, 2010). However any motion capture system should also incorporate mandible movement. An example is shown in Figure 13 whereby 4 spheres have been attached to an upper and lower framework, which is then attached to upper and lower teeth using two orthodontic brackets. Movement of the spheres in space will determine the trajectory of mandibular movement. Documenting this movement will be useful to plan the path of opening and closure of the jaw during surgery for individuals presenting with facial, trauma, oro-facial cancer and facial disharmony. All that is needed is a CBCT and at least 3 spheres located to the upper and lower dentition. The reliability of this system is generally within 1mm. An example is shown of an individual with bilateral fractures of the condyle and instead of the condyle articulating in the glenoid fossa the broken fragment is seen articulating with the zygomatic arch (Figure 13).

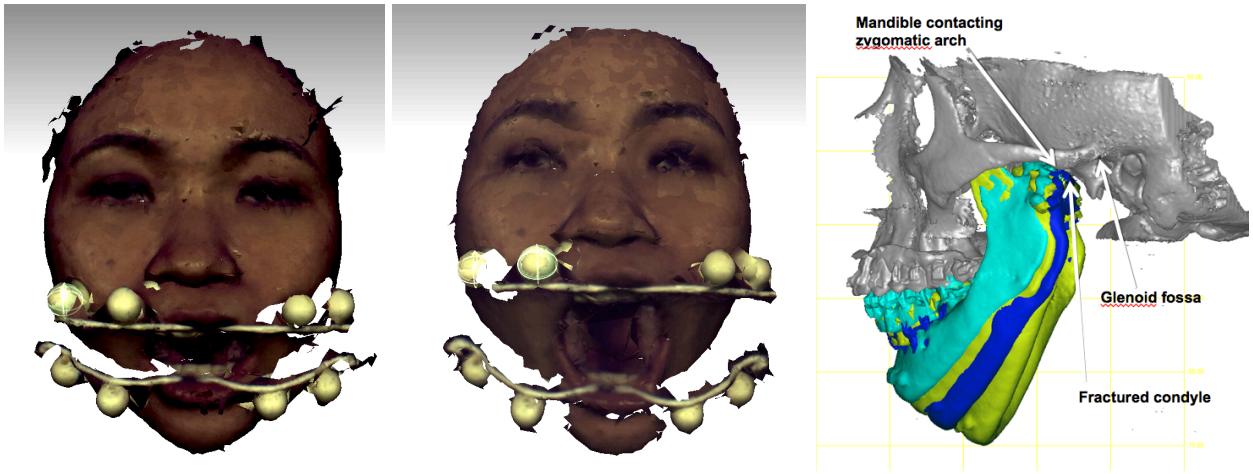

Figure 13 Tracking movement of the mandible using 4 spheres on a frame attached to upper and lower teeth (left 18mm opening; middle 42mm opening). The image on the right tracks mandibular movement for an individual with bilateral fractures of the condyle whereby the mandible pivots on the zygomatic arch as oppose to the condyle articulating with the glenoid fossa (right).

Refinement of techniques

Registration

It is often the case in medical imaging that important information is contained in more than one image (ensemble). A practical example of this would be latitudinal or longitudinal ensembles of facial 3D surface scans, obtained with surface scanners which are becoming a common and a valuable diagnostic tool. It is convenient to refer to 2D and 3D images, as well as surface scans, henceforth as simply “images”.

Typically, analysis of image ensembles involves construction of some statistical model. In contrast to hand-crafted models, which are inevitably inflexible and often inaccurate, modern statistical modelling methods allow for automatic construction of models directly from data. Before any meaningful analysis, statistical or otherwise, can be performed on an ensemble of images, correspondences between analogous parts of the images, across the entire ensemble, must first be established. This is accomplished by a procedure called *registration.* In other words, registration is a necessary prerequisite to extracting and aggregating useful information from an ensemble of images.

The methods for registration are classified according to the nature and modality of imagery to which they are applicable, according to the separation of samples (spatial, temporal, or both), by interactivity (manual, semi-automatic, automatic), by feature understanding (sparse, or feature-based, as opposed to dense, or area-based), by the model of admissible deformations, by multiplicity paradigm (pairwise or groupwise), and other properties (Sidorov, 2010).

Manual registration of large ensembles of images is tedious and error prone – while humans can

easily determine correspondences between salient features (*e.g.* eyes), they fail to establish correspondences between points in featureless regions (*e.g.* cheeks). Further, while manual annotation of 2D imagery is easily possible, in three dimensions it becomes prohibitively difficult for practical reasons. Hence, advances of computer vision are employed to perform registration tasks automatically.

Here, we briefly address automatic dense non-rigid groupwise registration applied to craniofacial 3D surface scans. Principal registration problems are: to register an ensemble of temporally separated images of the same subject (over various lengths of time: e.g. video of a person speaking; longitudinal study of growth over several years), and to register ensembles of images of several subjects, termed intra- and inter- subject registration accordingly.

Let us call what is actually observed by the imaging device (or the eye) the *appearance* of an image. Changes in appearance result from variations in the shape of the object e.g. deformation of the face during function, and from variations in the *texture* of the object e.g. blushing, shadows and facial hair. Both factors are usually present when images are obtained from different subjects. Changes in appearance due to variations in shape are typically highly non-linear and a priori unpredictable – simple changes in shape may cause complicated changes in appearance.
The purpose of registration is to determine the underlying deformation process that leads to the observed changes in appearance, and so determine how every point in one image is transformed into the analogous point in another image.

Depending on the range of admissible deformations, registration methods are roughly subdivided into *rigid* and *non-rigid*. Rigid methods crudely align the samples together, by computing global rigid transformations that bring all samples into alignment. Non-rigid methods allow for more general, local deformations to be recovered; this, however, comes at a much higher computational cost, as a substantially larger search space has to be explored. Some modern algorithms (Sidorov, 2009, Sidorov, 2011) explore the space of all possible deformation models in addition to exploring the space of parameters of a particular model, when searching for optimal correspondences.

Traditionally, when registering an ensemble of images, one image would be chosen as a "reference" and a pairwise registration method would be applied repeatedly to establish correspondences between the reference image and every other image in the ensemble, so establishing the correspondences between all pairs of images via the intermediate reference (the problem of registering a *pair* of images has been well-researched (Zitova 2003)). However, it has been recently shown (Cootes 2010, Sidorov 2009, Sidorov 2011) that this approach is suboptimal. Indeed, in such approaches the results is inevitably biased to the choice of the reference image;

and an unfortunate choice of the reference, for example one that is uncharacteristic of the rest of the ensemble, complicates matters further. More importantly, it has been shown (Cootes 2010, Sidorov 2009, Sidorov 2011) that a superior paradigm is to utilise as much information from the *entire* ensemble, rather than from only a pair at a time. Only by considering multiple examples simultaneously can corresponding structures be reliably identified. Registration methods that operate on this principle are called *groupwise*. Typically (Cootes 2010, Sidorov 2009, Sidorov 2011), groupwise registration amounts to constructing a common reference model of texture (to account for the variation in texture) and computing a set of models of deformation such that variation in the ensemble can be parsimoniously explained in terms of applying computed deformations to the model of texture. Accuracy and reliability of modern groupwise registration methods is typically higher than that of the pairwise registration, and higher than that of manual annotation (especially for relatively featureless imagery).

The problem of registration is ill-defined in the sense that there is no obvious criterion for optimality of registration results. Typically, the aim is to find a model of the underlying deformation process such that it best explains the changes of appearance in the *simplest* possible way.
Having registered the samples (that is, having found, for every point in each sample, the corresponding positions of the analogous points in every other sample), one can perform statistical analysis on the corresponding features.

To illustrate the usefulness of inter-subject registration, we took a corpus of 32 facial scans of different individuals, applied our registration algorithm to it (the evolution of the reference model is illustrated in Figure 8) and, having found the dense correspondences, computed a generative appearance model (Cootes 1998). The principal modes of variation, automatically found by registration and statistical modelling, are shown. We can use these registration techniques to explore facial expressions and speech.

a) Example different surfaces from the inter-subject dataset.

b) Evolution of the texture model in the flat parametric space as the registration progresses

c) Same as row above showing mean surface and texture in 3D

d) The three most significant modes of appearance variation automatically found by registration and statistical modelling.

Figure 8 Illustrates the evolution of the reference model; a) shows the original data; b) the texture model in the flat parametric space; c) mean surface and texture in 3D; d results - the three most significant modes of appearance variation automatically found by registration and statistical modelling.

Determination of the orientation of facial muscle fibres

Previously we used average estimates for facial muscle positioning, however each individual has different muscle masses and different origins and insertions. The manner in which a muscle delivers mechanical force is strongly dependant on its fibrous architecture has been understood for some time (Bovendeerd et al, 1994). Thus, to improve the understanding of subject-specific muscle mechanics, accurate estimations of fibre orientation must first be obtained *in vivo*. Some of the first successful non-invasive techniques worked by inspection of muscle fibre striation patterns visible through high-resolution structural MRI (Engstrom et al, 1991). Unfortunately, within MRI, not all muscles produce visible striations at feasible image resolutions and so, with the lack of any other inherent orientational information within structural MRI, such approaches were limited to the study of large muscles. It was not until the introduction of diffusion-weighted MRI (DW-MRI) (Steskal et al, 1965) that we could begin to probe tissue microstructure and begin to retrieve voxel-wise orientational information.

In principle, DW-MRI measures the rate of diffusion of water along a given orientation within a volume of interest. At first glance this appears disconnected from the retrieval of *in vivo* muscle fibre orientations; however, it was noticed that the particular cellular organisations (i.e. regularly arranged elongated fibrous cells) would produce distinct variations in the rate of diffusion of water relative to their macroscopic orientation. In other words, water may diffuse faster along a fibre than across fibres because it will encounter fewer hydrophobic cellular boundaries per unit length; in doing so this produces a measurable, modellable, diffusion anisotropy. From these observations various techniques were developed to turn raw directionally encoded 4D DW-MRI images into voxel-wise estimates of fibre orientation (Figure 14).

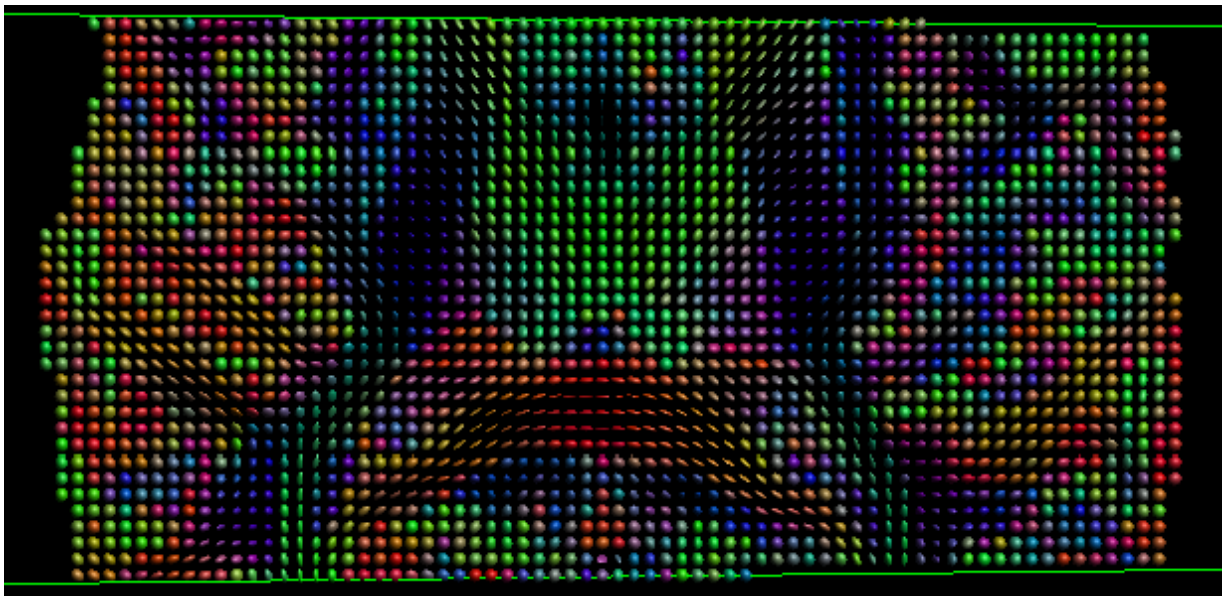

Figure 14 Voxel-wise estimates of fibre orientation retrieved through DT-MRI (Ellipsoidal representation). Image depicts a slice through the human brain. Direction is encoded through colour with blue representing orientations into and out of the plane, green forwards/backwards and

red left/right (otherwise known as directionally encoded colour)

One of the earliest, and potentially still the most popular of such techniques is Diffusion Tensor MRI (DT-MRI) (Basser et al, 1994). DT-MRI model assumes that fibrous diffusion can be modelled as a three-dimensional Gaussian diffusion tensor (i.e. an ellipsoid with the axis of greatest diffusion pointed down the fibre trajectory); by fitting this model to observed DW-signals, Eigen-analysis can reveal fibre orientation (the first Eigenvector) and a host of other useful quantitative parameters such including Fractional Anisotropy (FA), a ratio of longitudinal to radial diffusion (provided by the Eigenvalues) that might be useful to in the analysis of tissue integrity (Basser and Pierpaoli, 1996).

A logical step from voxel-wise measurements of orientation is to attempt to retrieve some representation of connectivity; to determine where a particular fibrous structure begins, where it ends and the path it follows along the way. To achieve this goal we employ a class of techniques collectively known as tractography (Basser et al, 2000). An *extremely* basic algorithm would be as follows: Position seed points in a regular grid across the target image, from each seed point, anchor two streamlines (remembering that fibres are axially-symmetric). Each streamline takes the orientation of its host voxel (or its inverse) and follows that path until reaching a boundary with a new voxel; checking the angle between its own orientation and the dominant orientation within the new voxel, a streamline will either (1) terminate if the angle is above a predefined threshold or (2) proceed through the new voxel taking on that voxels orientation until it reaches another voxel boundary and repeats the process. Once all streamlines have terminated or reached an image boundary, those sharing a common start point can then be joined to create a single coherent path. In this way a streamline can follow an orientationally coherent string of voxel-wise orientations while filtering out un-natural reconstructions (it is highly unlikely that a muscle fibre will deviate more than 35-40^{o} per 2-3mm step). The streamline can then be rendered as a 3D line with vertices at visited voxel boundaries, facilitating a more intuitive visual inspection. In reality such a simplistic approach would never be used, modern tractography will often employ techniques such as fibre orientation interpolation (placing vertices at fixed separations and computing point specific estimates of fibre orientation), probabalistic filtering (Parker et al, 2003) (to filter out erroneous streamlines) and support for more complicated DW-signal processing models (to be discussed shortly). An example of DT-MRI based tractography visualizing all tracts passing through the image slice is depicted in Figure 15.

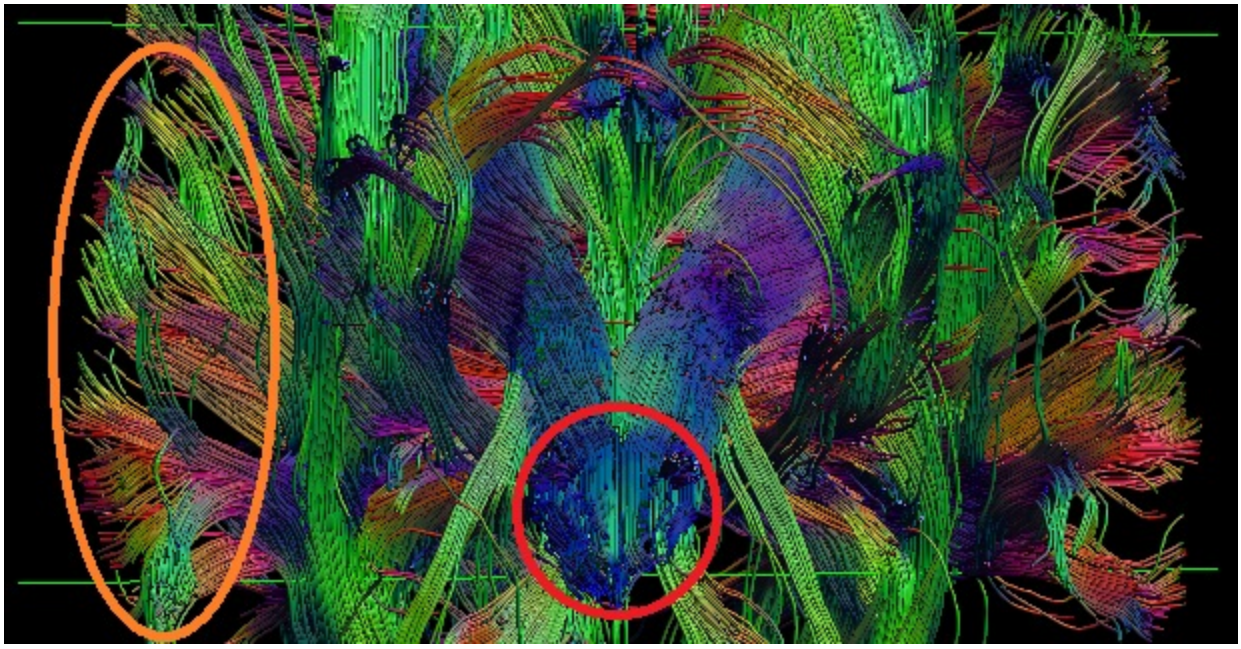

Figure 15 Result of DT-MRI based tractography displaying all tracts originating from or traversing through the slice of human brain depicted in Figure 14. Easily identifiable structures include sections of the brain stem (red) and *corpus callosum* (orange). Note that is far easier to identify connectivity through inspection of tractography than through voxel-wise data alone.

Unfortunately, DT-MRI is not without limitations. While DT-MRI derived estimates of fibre orientation can generally be considered reliable in voxels containing a single axially aligned fibre population, the tensor model is unable to resolve the 'crossing-fibres' problem that occurs when a voxel intersects two or more non-collinear fibre populations (Alexander et al, 2001). This is generally not a problem with larger muscles (relative to voxel dimensions) – explaining successful applications of DT-MRI to large muscle groups; legs (Heemskerk et aL, 2010; Kan et al, 2009), heart (Zhukov and Barr 2003; Kim et al, 2005) where one can derive important biomechanical properties such as the pennation angle (Heemskerk et al, 2005; Damon et al, 2002) – however as muscle size decreases relative to the size of a voxel, the frequency of intra-voxel orientational complexity increases (Figure 16) and thus the tensor model fails more frequently.

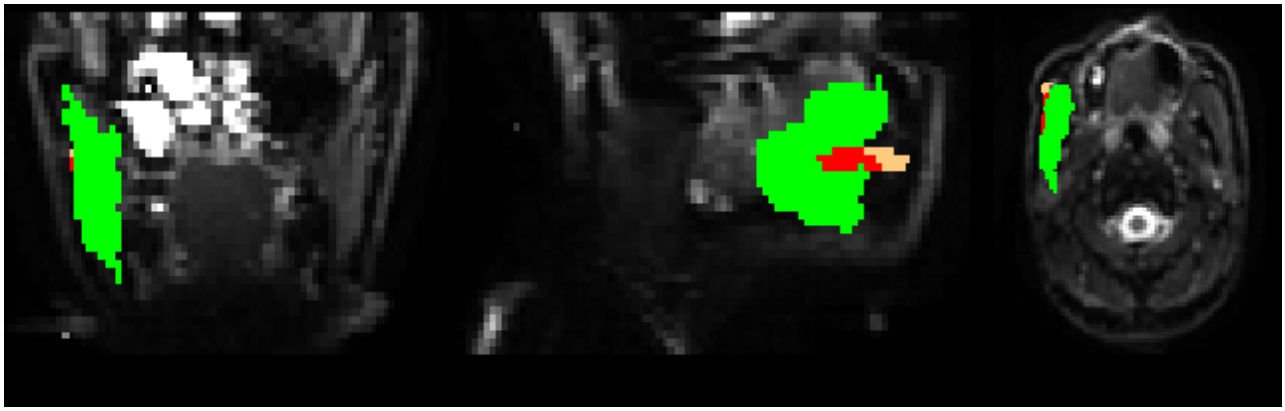

Figure 16 A demonstration of crossing-fibres. Here we have segmented visible portions of the *masseter* (green) and risorius (pink), red denotes shared voxels. Note that the largest portion of the

risorius lies within this shared region and thus the majority of the muscle would not be retrievable through DT-MRI. The *masseter* on the other hand is relatively easy to reconstruct, its relative size limits the effect of crossing fibre errors to smaller portions of its total volume.

Consequentially, when examining complex fibre architecture e.g. the tongue (Kim et al, 2005), successful DT-MRI often requires an image resolution that is not practical *in vivo* on clinical scanners (mostly due to SNR considerations at low field strengths 1.5-3T).

The challenge for muscle reconstruction in particular originates from the shorter T_2 of muscle fibre (35-45ms depending on activity (Rumeur et al, 1994)) in comparison to that of white matter (80ms) where study of complex fibre architecture is more prevalent. The resultant additional T_2 weighted signal losses, in combination with other factors more frequently encountered in *in vivo* studies of muscle (such as geometric distortions generated by magnetic inhomogeneities due to nearby air-tissue boundaries (Morgan et al, 2004)), imposes greater restrictions on voxel dimensions to ensure that the diffusion-weighted signal intensities are above the Rician noise floor (Jones and Basser, 2004). While white matter studies may reliable image at high resolutions, SNR considerations with *in vivo* muscle have typically forced use of a coarser 3 x 3 x 3mm resolution (our own situation) or lower.

Where DT-MRI has been applied to muscle structure *in vivo*, e.g. Gilberts study of the human tongue (Gibert and Napadow, 2005), SNR considerations forced a spatial resolution of 3 x 3 x 6-8mm. This coarse resolution then prevented the extraction of meaningful fibre orientations and instead forced a reliance on fractional anisotropy to imply structure – i.e. voxels with low anisotropy imply the presence of crossing fibre, from which inferences can be made through comparison with classical anatomy. Compared to later work by the same author (Gibert et al, 2006), which achieved successful lingual core tractography through diffusion spectrum imaging (DSI (Wedeen et al, 2005), one of many newer techniques designed to resolve crossing-fibres) of an *ex vivo* sample at voxel volumes ranging from 2 to 4 mm^3, it is clear that *in vivo* DT-MRI lacks the fidelity required to provide accurate subject specific biometric information. Unfortunately the high b-values required for DSI (a diffusion weighting affecting the weight of DW-signal attenuation with respect to measured diffusion weight) would result in unacceptably low *in vivo* SNR throughout the cranial-facial region on clinical hardware.

Constrained spherical harmonic deconvolution (CSHD (Tournier et al, 2004)) provides one possible way forward. However, despite the increasing number of applications of CSD to white matter, use on other fibrous tissue is largely undocumented (either *in* or *ex vivo*). The principle assumption of all spherical deconvolution approaches (numerous examples exist) is that the fibre orientation distribution function (i.e., a set of vectors describing the principle orientations of fibrous

tissue within the voxel) can be obtained through deconvolution of a 'common' single fibre response function (a representation of a DW-signal produced by a single-fibre population of the same tissue type) from the observed DW-signal – spherical deconvolution is no longer limited to one orientation per voxel. In practice, this common response function is not known *a priori* and thus an estimated/simulated fibre response must be used. Selection of an appropriate response is particularly important when applying CSDH as limitations inherent to its spherical harmonic data representation make it particularly unforgiving of errors at this point (Figure 17 left) (Parker and Jones, 2011). Fortunately however, our group has devised a simple, yet effective, automated response function selection technique (Parker and Jones, 2011) allowing us to apply CSHD with reasonable success, achieving anatomically viable reconstructions of the *Temporalis* (Figure 17 right), *Massetter* (Figure 18a)*, Buccinator* (Figure 18b)*, Risorius* and other smaller muscles where data quality permits (Figure 19).

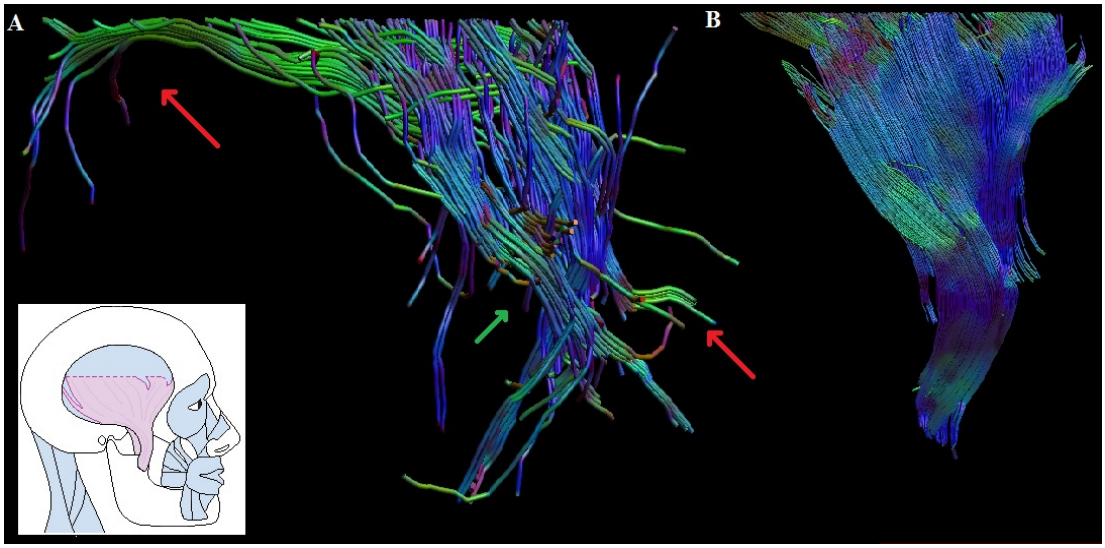

Figure 17 The effects of calibration on CSHD derived estimates of fibre orientation, a look at the *temporalis* muscle. An example of inappropriate calibration (the selected response function was of higher anisotropy than muscle tissue), typical errors include spurious fibre tracts with no basis in anatomy (marked red) and premature tract termination, especially in regions with higher curvature (marked green) (left). Tractography applied through the same volume as A, but with appropriate CSHD response function selection. Note that the reconstruction appears fuller in general, premature tract termination is greatly reduced and additional detail is visible at the muscles insertions into the mandible. Tractography at the upper edge is prematurely terminated in both A and B due to limited image coverage (right).

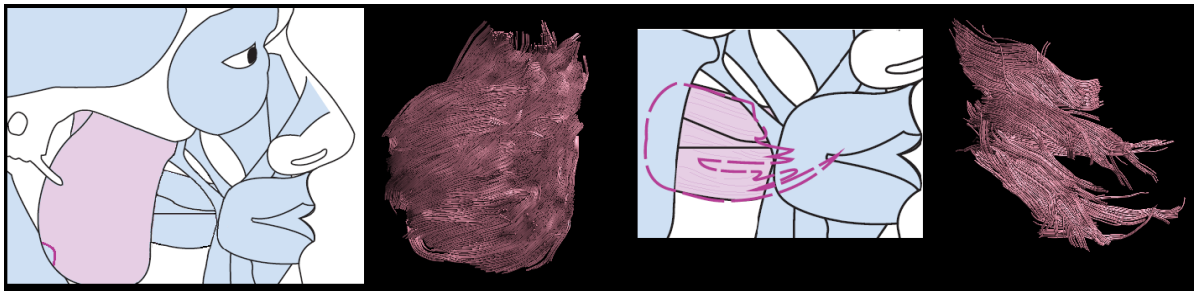

Figure 18 Example of a near complete *masseter* muscle reconstruction achieved through CSHD tractography (left). Example of a partial *buccinator* reconstruction, while image distortion within the cheek prevents a complete reconstruction crossing fibre resolution has been successfully achieved at the *masseter-buccinator* intersection (leftmost segment of the image) and the three main muscle components are clearly distinguishable (right).

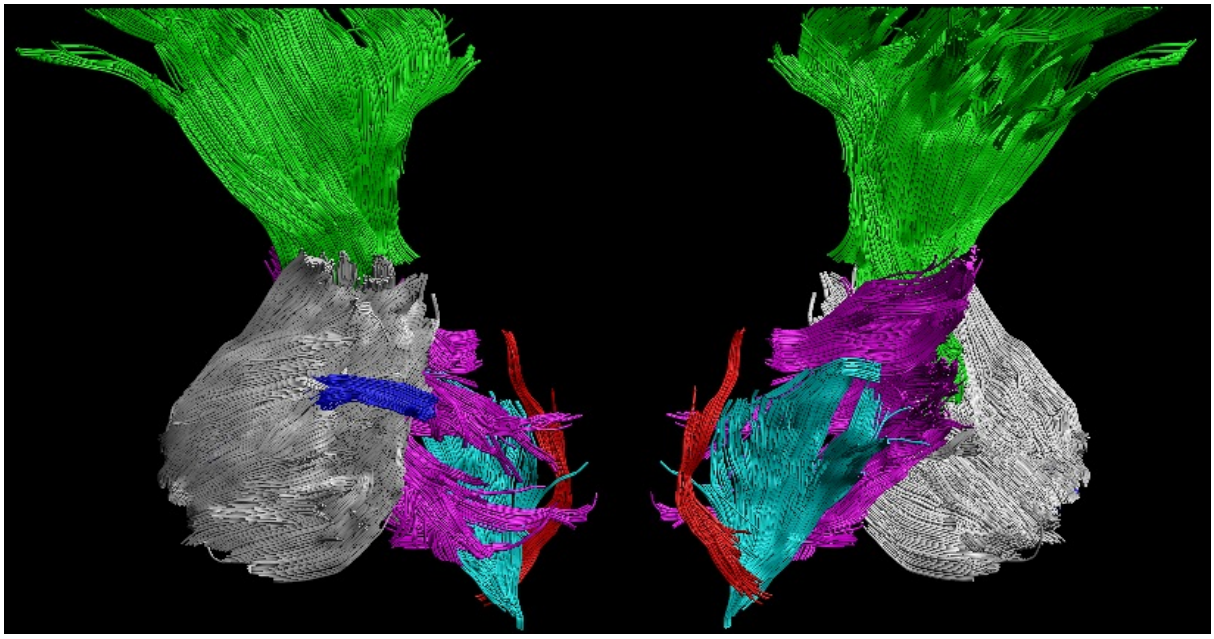

Figure 19 Selection of muscles shown in context. Green: *Temporalis*, Grey: *masseter*, Purple: *buccinator*, Blue: *risorius*, Cyan: *genioglossus*, Red: *depressor/levator anguli oris.* Unfortunately as we examine lower cranial-facial regions, DW-signal quality is such that reliable reconstruction is no longer achievable.

While advances have been made towards the signal-processing end our pipeline, image acquisition still remains problematic. Of the available imaging coils within our laboratory, the 8 channel brain imaging array provides the best coverage of our area of interest but, understandably, being optimized for brain imaging, tends to suffer from signal roll-off towards the below the subjects eyes. In combination with previously mentioned geometric distortions and T_2 related signal losses, data quality within the lower regions, particularly within the cheeks, about the lips and within the mandible can be particularly poor, resulting in incomplete or missing tractography. We are hopeful that with the addition of a new purpose built RF coil and introduction of a susceptibility matched medium into the subject's oral cavity, data quality will improve.

Conclusion

There are many genetic and non-genetic factors that influence facial shape and it is likely that further genotype and phenotype associations as well as environmental influences will be discovered as soon as larger 3D facial databases combined with genetic information become established. Appreciating individual facial features is important when evaluating changes as a result of growth and surgical interventions. A simple example of this is when a scalpel incision is made on the surface of the skin. The clinician often examines the lines on the skin surface and if the incision is made in line with the skin creases (Langer lines) scarring is often less visible as opposed to an incision made perpendicular to Langer lines. In the case of correcting facial disharmony the vast majority of surgery is performed intra-orally with minimal "invisible" scarring. However repositioning the bony surgical fragments will have an effect on the shape of the surface tissues and clinicians need to define the surface morphology and how the specific morphologies change with the magnitude of movement and spatial positioning. Surprisingly, with the wide variation in facial features, simple classifications such as, long/short, thin and wide still persist for individual facial features and shape is often ignored. Further work is needed to provide data for valid constituent modelling and to detail changes in the soft tissues during function. Nevertheless employing average parameters for soft tissues has provided an accurate model to predict facial surgery. Methods for automatic construction of craniofacial appearance models will in the future underpin much of craniofacial research, including realistic modelling of influences of non-invasive and invasive treatment modalities, management of facial injuries, predicting the effects of ageing, simulation of surgical intervention, post-surgical evaluation of a patient's appearance leading to the optimisation and refinement of surgical procedures. It is hoped that these significant advances will find their way into routine clinical practice in the near future.

References

Alexander A.L., K.M. Hasan, M. Lazar, J.S. Tsuruda, D.L. Parker. 2001. Analysis of partial volume effects in diffusion-tensor MRI. Magnetic Resonance in Medicine. 45(5):770-780.

Basser P.J., C. Pierpaoli. 1996. Microstructural and physiological features of tissues elucidated by quantitativediffusion-tensor MRI. Journal of Magnetic Resonance 111:209-219

Basser P.J., J. Mattello, D. Lebihan. 1994. Estimation of the effective self-diffusion tensor from the NMR spin echo. Journal of Magnetic Research. 103:247-254

Basser P.J., J. Mattiello, D. LeBihan. 1994. MR Diffusion Tensor Spectroscopy and Imaging. Biophysical Journal. 66:259-267

Basser P.J., S. Pajevic, C. Pierpaoli, J. Duda, A. Aldroubi. 2000. In Vivo Tractography Using DT-MRI Data. Magnetic Resonance in Medicine 44:625-632

Beldie L, Walker B, Lu YT, Richmond S, Middleton J. Finite element modelling of maxillofacial surgery and facial expressions – a preliminary study. The International Journal of Medical Robotics

and Computer assisted Surgery. Volume 6, issue 4, December 2010, Pages: 422-430.
Bhatia SN, Leighton BC Manual of Facial Growth: A Computer Analysis of Longitudinal Cephalometric Growth Data (Oxford Medical Publications) 1993.
Bovendeerd PH, JM Huyghe, T Arts, DH Van Campen DH,RS Reneman. 1994. Influence of endocardialepicardial of muscle fibres on left ventricular wall mechanics. Journal of Biomechanics. 27:941-951
Bryant JA, Drage NA, Richmond S. Study of the scan uniformity from an i-CAT cone beam computed tomography dental imaging system. Dentomaxillofac Radiol. 2008 Oct;37(7):365-74.
Cohen MM, Malformations of the Craniofacial Region: Evolutionary, Embryonic, Genetic, and Clinical Perspectives. American Journal of Medical Genetics (Semin. Med. Genet.) 115:245–268 (2002)
Cootes TF, C. J. Twining, V. S. Petrovic, et al. “Computing accurate correspondences across groups of images”. IEEE Transactions on Pattern Analysis and Machine Intelligence, volume 32(11):pages 1994–2005, 2010.
Cootes TF, G. J. Edwards, C. J. Taylor. “Active appearance models”. In Proceedings of the European Conference on Computer Vision, pages 484–498, 1998.
Damon B.M., Z. Ding, A.W. Anderson, A.S. Freyer, J.C. Gore. 2002. Validation of diffusion tensor MRI-based muscle fiber tracking. Magnetic Resnonance in Medicine. 48: 97-104.
Djordjevic J, Richmond S, Toma A, Zhurov A. Three-dimensional facial morphology and insulin sensitivity – a longitudinal study. 7th International Orthodontic Congress, Sydney, Australia, February 6-9, 2010
Drage N, Rout J, Diagnostic Imaging, in Three-Dimensional Imaging for Orthodontics and Maxillofacial Surgery, Ed Kau Ch and Richmond S. Wiley Blackwell, 2010, 978-0813806143
Dryden, I. L. & Mardia, K. V. (1998) Generalised Procrustes Methods. In Barnett, V., Bradley, R. A., Cressie, N., Fisher, N. I., Johnstone, I., Kadane, J. B., Kendall, D. G., Scott, D. W., Bernard, B., Smith, A. F. M. & Teugels, J. L. (Eds.) Statistical Shape Analysis. Chichester, Wiley.
Engstrom CM, GE Loeb, JG Reid, WJ Forrest, L Avruch. 1991. Morphometry of the human thigh muscles. A comparison between anatomical sections and computer tomographical and magnetic resonance images. Journal of Anatomy. 176:139-156
Evans DM, Paternoster L, Toma AM,Zhurov AI, Kemp JP, St. Pourcain B, Timpson NJ, McMahon G., Ring SM, Smith GD, Richmond S. American Society of Human Genetics, 2011 Montreal. Genome-wide association study of three-dimensional facial morphology identifies a variant in the PAX3 gene responsible for normal variation in face shape.
Farkas, L. (1993) Anthropometry Of The Head And Face, New York, Raven Press.
Gilbert R.J., V.J. Napadow. 2005. Three-dimensional muscular architecture of the human tongue determined in vivo with diffusion tensor magnetic resonance imaging. Dysphagia 20:1-7
Gilbert R.J., V.J. Weeden, L.H. Magnusson, T. Benner, R. Wang, G. Dai, V.J. Napadow, K.K. Roche. 2006. Three-Dimensional Myoarchitecture of the bovine tongue demonstrated by diffusion

spectrum magnetic resonance imaging with tractography. The Anatomical Record Part A. 288A:1173-1182
Heemskerk A.M., G.J. Strijkers, A. Vilanova, M.R. Drost, K. Nicolary. 2005. Determination of Mouse Skeletal Muscle Architecture Using Three-Dimensional Diffusion Tensor Imaging. MRM 53:1333-1340.
Heemskerk A.M., T.K. Sinha, K.J. Wilson, Z. Ding, B.M. Damon. 2010. Repeatability of DTI-based skeletal muscle fibre tracking. NMR in Biomedicine. 23(3):294-303.
Henderson J, Granell R, Heron J, Sherriff A, Simpson A, Woodcock A, Strachan DP, Shaheen SO, Sterne JA. Associations of wheezing phenotypes in the first 6 years of life with atopy, lung function and airway responsiveness in mid-childhood. Thorax. 2008 Nov;63(11):974-80. Epub 2008 Aug 4.
Hill AV (ed) The heat shortening and the dynamic constants of muscle. Proc R Soc London B 1938; 126: 136.
Hundley WG, Bluemke DA, Finn JP, et al. ACCF/ACR/AHA/NASCI/SCMR 2010 expert consensus document on cardiovascular magnetic resonance: A report of the American College of Cardiology Foundation Task Force on Expert Consensus Documents. Circulation. 2010;121(22):2462-2508.
Jones D.K., P.J. Basser. 2004. Squashing peanuts and smashing pumpkins: How noise distorts diffusion-weighted MR data. Magnetic Resonance in Medicine 52:979-993.
Kan J.H., M.H. Anneriet, Z. Ding, A. Gregory, G. Mencio, K. Spindler K, B.M. Damon. 2009. DTI-based muscle fibre tracking of the quadriceps mechanism in lateral patellar dislocation. Magnetic Resonance in Medicine 29(3):663-670
Kang SH, Kim DK, Seo KM, Seo JH. Usefulness of videofluoroscopic swallow study with mixed consistency food for patients with stroke or other brain injuries. J Korean Med Sci. 2011 Mar;26(3):425-30.
Kau CH, Three-dimensional surface acquisition systems for facial analysis, in Three-Dimensional Imaging for Orthodontics and Maxillofacial Surgery, Ed Kau Ch and Richmond S. Wiley Blackwell, 2010, 11-28, ISBN 978-0813806143
Kau CH, Richmond S, Zhurov A, Ovsenik M, Tawfik W, Borbely P, English JD. Use of 3-dimensional surface acquisition to study facial morphology in 5 populations. Am J Orthod Dentofacial Orthop. 2010 Apr;137(4 Suppl): S56.e1-9.
Kim S., G. Chi-Fishman, A.S. Barnett, C. Pierpaoli. 2005. Dependence on diffusion time of apparent diffusion tensor of ex vivo calf tongue and heart. Magnetic Resonance in Medicine 54(6):1287-96.
Kim DS, Choi SC, Lee SS, Heo MS, Huh KH, Hwang SJ, Yi WJ. (2010). Correlation between 3-dimensional facial morphology and mandibular movement during maximum mouth opening and closing. Oral Surg Oral Med Oral Pathol Oral Endod **110**:648-656
Kohn, LAP. The Role of Genetics in Craniofacial Morphology and Growth. Annual Review of Anthropology 20, 261-278(1991).

Lu YT, Beldie L, Walker B, Richmond S, Middleton J. Parametric study of a Hill-type hyperelastic skeletal muscle model. Proceedings of the Institution of Mechanical Engineers. Part H: Journal of Engineering in Medicine. Volume 225, issue 5, May 2011, Pages: 437-447.

Lundström A. Nature versus nurture in dentofacial variation. 1984 European Journal of Orthodontics, 6, 77-91.

Martin CJA, Alarcon JA, Palma JC. (2000). Kinesiographic study of the mandible in young patients with unilateral posterior crossbite. American Journal of Orthodontics and Dentofacial Orthopedics 118: 541-548.

Mishima, K., Yamada, T., Sugii, A., Matsumura, T. & Sugahara, T. (2009) Application Of A Novel Method To Analyse Lip Motion Of Cleft Lip Patients Before And After Lip Repair. Dento-Maxillo-Facial Radiology, 38, 232-8.

Morgan PS, Bowtell RW, McIntyre DJO, Worthington BS. 2004. Correction of spatial distortion in EPI due to inhomogeneous static magnetic fields using the reversed gradient method. Journal of Magnetic Resonance Imaging 19(4):499-507

Nooreyazdan, M., Trotman, C. A. & Faraway, J. J. (2004) Modeling Facial Movement: Ii. A Dynamic Analysis Of Differences Caused By Orthognathic Surgery. Journal Of Oral And Maxillofacial Surgery, 62, 1380-6.

Okudaira, M., Ono, T., Kawamoto, T. & Moriyama, K. (2008) Three-Dimensional Analysis Of Lower Lip Movement During Articulation In Subjects With Mandibular Prognathism. Orthodontic Waves, 67, 93-103.

Parker GJM, Haroon HA, Wheeler-Jingshott CAM. 2003. A Framework for a Streamline-Based Probabilistic Index of Connectivity (PICo) Using a Structural Interpretation of MRI Diffusion Measurements. Journal of Magnetic Resonance Imaging 18:242-254

Parker GD, Jones DK. 2011a. Fibres at the Magic Angle Generated by Inappropriate Calibration (MAGIC). Proc. ISMRM 2011: 1921

Parker GD, Jones DK. 2011b. Towards Automated Modelling of Maxillofacial Musculature. Proc ISMRM 2011: 1916

Popat, H., Henley, E., Richmond, S., Benedikt, L., Marshall, D. & Rosin, P. L. (2010) A Comparison Of The Reproducibility Of Verbal And Non-Verbal Facial Gestures Using Three-Dimensional Motion Analysis. Otolaryngology - Head And Neck Surgery, 142, 867-872.

Popat, H., Richmond, S., Marshall, D. & Rosin, P. L. (2011) Facial Movement In 3 Dimensions: Average Templates Of Lip Movement In Adults. Otolaryngol Head Neck Surg, 145, 24-9.

Riolo ML, Moyers RE, McNamara JA, Hunter WS. An Atlas Of Craniofacial Growth (vol.2), Needham Press 1979.

Rumeur E.L.E., F. Carre, A.M. Bernard, J.Y. Bandard, P. Rochcongar, J.D.D.E. Certained. 1994. Multiparametric classification of muscle T1 and T2 relaxation times determined by magnetic resonance imaging. The effects of dynamic exercise in trained and untrained subjects. British Journal of Radiology 67:150-156

Saunders SR, Popovich F, Thompson GW, A family study of craniofacial dimensions in the Burlington Growth Centre sample, American Journal of Orthodontics, Volume 78, Issue 4, October 1980, Pages 394-403.
Richmond S, Beldie L, Lu Y, Middleton J, Walker B, Cronin A, Drage N, Zhurov A, Wilkinson C. Predicting and Managing Surgical Intervention in Craniofacial Disharmony – a Biomechanical Perspective. Three-Dimensional Imaging for Orthodontics and Maxillofacial Surgery, Wiley Blackwell, 2010, 180-197. ISBN 978-0813806143
Sidorov K, S. Richmond, D. Marshall. “An Efficient Stochastic Approach to Groupwise Non-rigid Image Registration”. In Proc. IEEE Conf. on Comp. Vis. and Pat. Rec. (CVPR '09), pages 2208—2213, 2009.
Sidorov K, S. Richmond, D. Marshall. “Efficient Groupwise Non-rigid Registration of Textured Surfaces”. In Proc. IEEE Conf. on Comp. Vis. and Pat. Rec. (CVPR '11), pages 2401—2408, 2011.
Sidorov K. “Groupwise Non-rigid Registration for Automatic Construction of Appearance Models of the Human Craniofacial Complex for Analysis, Synthesis, and Simulation”. PhD Thesis, Cardiff University, 2010.
Stjeskal EO, Tanner EJ. 1965. Spin diffusion measurements: spin echoes in the presence of time-dependent field gradient. J. Chem. Phys. 42:288-292
Toma AM, Zhurov AI, Playle R, Marshall D, Rosin PL, Richmond S. The assessment of facial variation in 4747 British school children. Eur J Orthod. 2011 Sep 20.
Tournier J.D., F. Calamante, D.G. Gadian, A. Connelly. 2004. Direct estimation of the fiber orientation density function from diffusion-weighted MRI data using spherical deconvolution, Neuroimage 23 pp. 1176-1185.
Wedeen V.J., P. Hagmann, W.I. Tsend, T.G. Reese, R.M. Weisskoff. 2005. Mapping complex tissue architecture with diffusion spectrum magnetic resonance imaging. MRM 54:1337-1386
Wood GD. 1979 Recording the opening and closing cycle of the mandible. British Dental Journal **146**: 305-309.
Zhukov L., A.H. Barr. 2003. Heart-Muscle Fibre Reconstruction from Diffusion Tensor MRI. Proceedings of the 14th IEEE Visualization Conference 0-7695-2030-8
Zhurov AI, Richmond S, Kau CH, Toma A, Averaging facial images. in Three-Dimensional Imaging for Orthodontics and Maxillofacial Surgery, Ed Kau Ch and Richmond S. Wiley Blackwell, 2010, 126-146, ISBN 978-0813806143
Zitova B, J. Flusser. “Image registration methods: a survey”. Image and Vision Computing, volume 21(11):pages 977–1000, 2003.